Physics Letters B 780 (2018) 227–232

Contents lists available at ScienceDirect

Physics Letters B

www.elsevier.com/locate/physletb

Enhanced collectivity in ^{12}Be

C. Morse [a,*], E.A. McCutchan [b], H. Iwasaki [c,d], C.J. Lister [a], V.M. Bader [c,d], D. Bazin [c], S. Beceiro Novo [c], P. Chowdhury [a], A. Gade [c,d], T.D. Johnson [b], C. Loelius [c,d], E. Lunderberg [c,d], E. Merchan [a], V.S. Prasher [a], F. Recchia [c], A.A. Sonzogni [b], D. Weisshaar [c], K. Whitmore [c,d]

[a] Department of Physics, University of Massachusetts Lowell, Lowell, MA 01854, USA
[b] National Nuclear Data Center, Brookhaven National Laboratory, Upton, NY 11973, USA
[c] National Superconducting Cyclotron Laboratory, Michigan State University, East Lansing, MI 48824, USA
[d] Department of Physics and Astronomy, Michigan State University, East Lansing, MI 48824, USA

ARTICLE INFO

Article history:
Received 30 May 2017
Received in revised form 10 February 2018
Accepted 2 March 2018
Available online 8 March 2018
Editor: D.F. Geesaman

Keywords:
Lifetimes
Nuclear transition probabilities
Collectivity

ABSTRACT

Electromagnetic quadrupole transition strength is a sensitive probe of the evolution of the structure of nuclei, particularly the competition between collectivity and magicity. We have performed a new lifetime measurement of the 2_1^+ state of ^{12}Be to study the interplay of these phenomena. The lifetime was measured with the Doppler Shift Attenuation Method using the γ-ray detector GRETINA. Excited states of ^{12}Be were produced via inelastic scattering at 55 MeV/nucleon, using several different targets to control for systematic uncertainties in the stopping powers. The lifetime is determined to be $\tau = 1.38 \pm 0.10(\text{stat}) \pm 0.19(\text{sys})$ ps, which is about half the previously reported value at twice the precision. The reduced transition strength deduced from this result is $B(E2; 2_1^+ \rightarrow 0_1^+) = 14.2 \pm 1.0(\text{stat}) \pm 2.0(\text{sys})\ e^2\,\text{fm}^4$, which supports the quenching of the $N = 8$ shell gap in ^{12}Be.

1. Introduction

The development of collective structures in light nuclei has long been the subject of attention in nuclear structure studies [1–3]. Recent experimental and theoretical work has greatly expanded the knowledge of light nuclear systems extending towards the neutron dripline [4–11]. Such insights are timely, as modern theoretical calculations are taking advantage of ever-increasing computational capabilities to reveal nuclear properties in impressive detail. Therefore, precise data from such nuclei are needed in order to evaluate these emerging nuclear models.

The beryllium isotopic chain is an iconic example of collectivity in nuclei, particularly clustering. This can be seen in ^{8}Be, which disintegrates into two α particles and clearly demonstrates its clustered nature [12]. While the heavier isotopes are bound against this decay mode, α structure breakup and neutron removal cross sections have shown that clustering persists even in these more neutron-rich systems [6]. Thus, the $N > Z$ beryllium isotopes can be considered to be 2α dumbbell-shaped nuclei surrounded by clouds of neutrons, possibly forming "nuclear molecules" where the neutrons play a role analogous to the electrons in atomic molecules [13]. Understanding the evolution of these nuclei as a function of neutron number, especially crossing the neutron magic number $N = 8$ and approaching the two-neutron halo nucleus ^{14}Be [14], has proven and continues to be a productive field of study.

A special case among the beryllium isotopes is the nucleus ^{12}Be. Located at the magic number $N = 8$, ^{12}Be embodies a tension between the deformed or clustering behavior displayed by the other beryllium isotopes and the tendency to revert to a spherical shape at the neutron-shell closure. Numerous investigations have been conducted to examine the structure of this unique system. It was revealed by γ-ray spectroscopy that the first excited state in ^{12}Be [15] lies at significantly lower energy than in ^{10}Be [16], at odds with the expectation that the $J^\pi = 2_1^+$ state should be relatively high in excitation energy in a closed-shell system. Inelastic proton scattering showed that the deformation length of ^{12}Be is slightly larger than that of ^{10}Be [17], and a recent measurement found that the proton radius of ^{12}Be is significantly larger than that of the lighter isotopes [8]. Finally, one-neutron knockout reactions revealed s and p spectroscopic factors with nearly equal magnitudes [18], and later even a significant d-wave contribution [19].

* Corresponding author at: 1 University Ave, Lowell, MA 01854, USA.
E-mail address: christopher_morse@uml.edu (C. Morse).

https://doi.org/10.1016/j.physletb.2018.03.004

Together, this evidence makes a strong case that the traditional spherical $N = 8$ shell closure is quenched in ^{12}Be.

Despite these studies, one metric of the nuclear structure of ^{12}Be remains ambiguous: the $B(E2; 2_1^+ \rightarrow 0_1^+)$ transition probability. Given the surprisingly low 2_1^+-state energy, the naïve expectation would be that the $B(E2)$ strength in ^{12}Be should be considerably higher than that in ^{10}Be. However, while the $B(E2)$ for ^{12}Be has been determined in a prior measurement to be $B(E2) = 8.0 \pm 2.2(\text{stat}) \pm 0.8(\text{sys})\ e^2\,\text{fm}^4$ [20], the uncertainty is large enough that it cannot be established whether it increases, decreases, or remains constant compared to ^{10}Be ($B(E2) = 9.2(3)\ e^2\,\text{fm}^4$ [21]). Resolving this ambiguity by more precisely determining the $B(E2)$ in ^{12}Be is therefore critical to gauge the competition between collectivity and the shell closure.

Here we present a new measurement of the 2_1^+-state lifetime in ^{12}Be in order to constrain the $B(E2; 2_1^+ \rightarrow 0_1^+)$ transition rate in this nucleus. The lifetime is the leading contribution to the uncertainty in the $B(E2)$, and was previously reported to be $\tau_{2_1^+} = 2.5 \pm 0.7(\text{stat}) \pm 0.3(\text{sys})$ ps, measured via the Doppler Shift Attenuation Method (DSAM) [20]. The previous experiment was well-optimized for ^{12}Be production and served as a demonstration of DSAM with fast radioactive beams, but suffered from poor statistical uncertainty. The present experiment follows a similar design, but with several key improvements to achieve better precision. Most significantly, the present experiment uses the Gamma Ray Energy Tracking In-beam Nuclear Array (GRETINA) [22] for γ-ray detection. Compared to the two Clover detectors used in the previous experiment, GRETINA is both significantly more efficient due to increased solid-angle coverage, and also allows for much more precise localization of γ-ray interaction points within the detectors. This allows for much better Doppler-reconstruction while keeping the detectors close to the target to retain the large solid-angle coverage. A recoil separator was also used in the present experiment in order to cleanly identify the nuclear reaction channel producing ^{12}Be and to determine the outgoing reaction product momenta, which complements the position resolution of GRETINA by further constraining the γ-ray emission angle. Finally, where the previous experiment used only one target to produce excited states of ^{12}Be, the present study uses three targets of varying thicknesses and materials. This is important in order to better understand and quantify systematic effects and uncertainties in this measurement, as DSAM depends critically on the stopping power of the target materials used to slow the excited ^{12}Be nuclei.

2. Experimental details

The experiment was performed at the National Superconducting Cyclotron Laboratory (NSCL) on the campus of Michigan State University. The Coupled Cyclotron Facility provided a primary beam of ^{18}O at 120 MeV/nucleon which was fragmented on a natural beryllium target to produce ^{12}Be. The resulting secondary beam was purified in the A1900 fragment separator [23] with the aid of an aluminum degrader and a momentum acceptance setting of 0.5%. The secondary beam had a purity of approximately 96% ^{12}Be at 55 MeV/nucleon and a typical rate of 1×10^5 pps. This secondary beam was transported to the experimental area where excited states were populated through inelastic scattering on several different targets. The scattered ^{12}Be nuclei were identified by energy-loss and time-of-flight in the S800 spectrometer [24]. Based on the particle positions and momenta measured in the focal plane detectors of the S800, the trajectories and velocities of the recoiling ^{12}Be nuclei as they exited the target were reconstructed on an event-by-event basis. For a typical beam spot size of about 1 cm, the accuracy of the reconstruction of the beam profile at the target is on the order of a few mrad for both the dispersive and non-dispersive angles, about 0.5 mm for the position in the non-dispersive direction, and about 1 part in 1000 in the kinetic energy [24].

The γ rays from ^{12}Be were detected with GRETINA, which consisted of seven detector modules each composed of four 36-fold electrically-segmented HPGe crystals. Analysis of the digitized pulses from the crystal segments allows the location of γ-ray interactions within the crystal to be determined, while the energy deposited is determined by the central contact. For events in which multiple interactions occurred, the interaction point was taken to be the one with the highest energy deposit, which has been shown to be a good approximation of the true first interaction point [25]. Doppler correction of the laboratory-frame γ-ray spectrum was performed event-by-event using the angle between the vector from the target to the interaction points measured in GRETINA and the after-target trajectories of the scattered nuclei determined by the S800, as explained in Ref. [25]. The velocity chosen for the Doppler correction was the after-target velocity, also measured event-by-event in the S800. Addback was performed within each detector module, so that the central contact energy of each crystal was summed in order to recover partial energy deposition events. Four of the seven GRETINA modules were placed at forward angles centered around 58° and three modules at 90° relative to the beam direction in the laboratory frame. However, because DSAM achieves its greatest sensitivity to excited-state lifetimes at far-forward and far-backward angles, the targets were shifted about 20 cm upstream (that is, in the opposite direction of the beam current) from the center of GRETINA, after which the detectors were centered around 30° and 50° in the laboratory frame, spanning an angular range from 20° to 70°.

^{12}Be has only three bound excited states: a 2^+ state at 2.1 MeV, a 0^+ state at 2.2 MeV, and a 1^- state at 2.7 MeV [9]. These excited states decay almost exclusively to the ground state (the 0_2^+ state decays directly to the ground state via an $E0$ transition 87.3(35)% of the time [9]). Thus the addback routine introduces minimal error from accidental summing of distinct γ rays but increases the photopeak yields by about 30%. Three separate targets were used to populate these excited states during the experiment in order to control for systematic effects from uncertainties in the stopping power of the target materials: a 2490-mg/cm^2 Ta target, a 1330-mg/cm^2 Ta target, and a 1410-mg/cm^2 Nb target. The γ-ray spectrum collected for the 2490-mg/cm^2 Ta target is shown in Fig. 1(a) and (b). Panel (a) shows the γ-ray spectrum as a two-dimensional plot in order to demonstrate the Doppler correction, with the γ-ray emission angle relative to the ^{12}Be recoil direction on the vertical axis and the Doppler-corrected γ-ray energy on the horizontal axis. The broad nature of the photopeaks is due to the short lifetime of the excited states, which primarily decay inside the target rather than in vacuum after exiting the target. Because the beam velocity used for Doppler correction is that which is measured after the target, the photopeaks are expected to have a vertical edge on the low-energy side due to decays at the back of the target, with a broad shoulder extending to higher energies due to decays which happen at a higher velocity inside the target. This shape can be clearly seen for the 2_1^+ and 1_1^- photopeaks labeled in Fig. 1(a). In contrast, the 511 keV peak marked by the * is a laboratory-frame photopeak, and does not show any Doppler-broadening. Fig. 1(b) is the projection of Fig. 1(a) onto the γ-ray energy axis. The $0_2^+ \rightarrow 2_1^+$ transition occurs for only 12.7(35)% of the 0_2^+-state decays [9], and is not observed due to the long mean lifetime of $\tau = 331(12)$ ns [26] for this state. The long lifetime results in the nuclei decaying over a wide range of distances after the target. This leads to a very wide distribution in Doppler-shifted en-

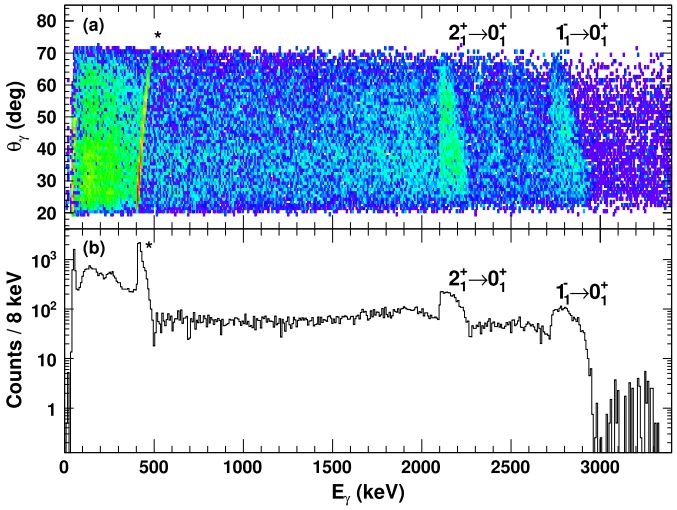

Fig. 1. (Color online) (a) The Doppler-corrected addback γ-ray spectrum collected with all GRETINA detectors from the excitation of ^{12}Be on a 2490-mg/cm^2 Ta target. The vertical axis shows the γ-ray emission angle relative to the recoiling ^{12}Be trajectory, and the horizontal axis shows the Doppler-corrected γ-ray energy. The γ rays from the decay of the 2_1^+ and 1_1^- states are labeled, while the * indicates 511 keV photons. (b) The same as (a), but projected onto the γ-ray energy axis.

ergies which is indistinguishable from background, and so no peak is observed from this transition in this fast-beam experiment.

The lifetime of the 2_1^+ state of ^{12}Be was determined using the DSAM technique described below. The present experiment used beam energies of several tens of MeV per nucleon, such that the excited nuclei do not stop in the targets and event-by-event particle identification is possible. The targets used in this experiment are thick, and excited states can be produced through inelastic scattering at any point in the target. As a consequence, the expected shape of the laboratory-frame γ-ray spectrum is not that of a narrow photopeak from the decay of stopped nuclei, with an extended tail due to decays of nuclei in-flight. Instead, all nuclei decay in-flight, and Doppler correction is applied to the observed γ-ray spectrum using the beam velocity $\beta = v/c$ after the target as measured in the S800. This β corresponds to decays which occur after the beam has left the target and maintains a constant velocity, which results in a narrow peak in the Doppler-corrected spectrum in analogy to the stopped peak in classic DSAM. Decays which occur before the nuclei exit the target will have a β larger than that used for Doppler correction, so that the Doppler shifts are only partially corrected for these decays. This results in a broadened component to the photopeak, which is analogous to the in-flight component in classic DSAM. In the present case, the GRETINA detectors are placed only at downstream angles, and the broadening occurs only towards higher energies such that the peaks are asymmetric. For extremely short-lived states such as the 1_1^- state ($\tau = 1.9$ fs deduced from Ref. [27]), all decays occur within the target and there is no after-target component. Instead, the average decay velocity corresponds to β roughly halfway through the target, which is higher than β measured in the S800 and causes the peak to shift towards higher energy. As the lifetime increases, more decays will occur after exiting the target, causing the after-target component to increase. The sensitivity to the lifetime is achieved through the ratio of the population of the after-target component relative to the population of the in-target component. For the 2_1^+ photopeak in Fig. 1, the lifetime is apparently significantly less than the transit time of the beam through the target (about 10 ps at NSCL beam velocities) due to the lack of a prominent after-target peak. However, the maximum of the peak occurs on the low-energy edge where the after-target component would be located, rather than being shifted towards higher energies. This indicates that a small after-target component is present and the method described here is sensitive even to this short lifetime.

3. Analysis

Lifetimes were extracted from the data with the aid of a Monte Carlo simulation code [28] based on the Geant4 [29] and ROOT [30] frameworks. The simulation package is designed for lifetime analyses and has been recently updated to include the description of the GRETINA detector geometry. Excited-state energies and lifetimes are used as inputs in order to reproduce the response function of GRETINA to the experimentally measured γ-ray spectrum. In addition, the simulation allows the measured beam properties to be described, and accepts a parameterized description of the reaction mechanism in order to match the experimental beam profile measured in the S800. The lifetime of the 2_1^+ state was varied between 0 ps and 3 ps in steps of 0.25 ps, while the lifetime of the 1_1^- state was kept fixed at 1.9 fs, as deduced from the $B(E1)$ value found for the $1_1^- \rightarrow 0_1^+$ transition [27]. Separate sets of simulations were performed for each of the three different targets used in the experiment.

Once a set of simulations was generated, it was fit to the experimental data along with an exponential background through a χ^2 minimization procedure. The shape of the background was determined by first fitting a wide energy region including the γ-ray transitions, and then fixing the parameters of the exponential background. The intensity of the $1_1^- \rightarrow 0_1^+$ transition was also fixed at this point, as it does not contribute to the determination of the 2_1^+-state lifetime except through the Compton background, leaving only the intensity of the $2_1^+ \rightarrow 0_1^+$ transition as a free parameter. The fit was then evaluated over the energy range covered by the 2.1-MeV photopeak, and the resulting χ^2 per degree of freedom (χ^2/N) saved. This process was repeated for each simulated 2_1^+-state lifetime, and the lowest χ^2/N taken to be the lifetime. Fig. 2 shows the results of this fitting procedure for (a) the 2490-mg/cm^2 Ta target, (b) the 1330-mg/cm^2 Ta target, and (c) the 1410-mg/cm^2 Nb target, with the best-fit simulations (red solid lines) overlaying the data. The shaded regions indicate the energy range used to determine the 2_1^+-state lifetime. The insets show the distribution of reduced χ^2 values as a function of simulated lifetime. The lifetimes determined from each target data set were (a) 1.34(17) ps, (b) 1.67(16) ps, and (c) 1.14(18) ps, where the uncertainties are only statistical. As a consistency check, a similar analysis was performed for the $1_1^- \rightarrow 0_1^+$ transition, allowing the lifetime of the 1_1^- state to vary. The lifetime was found to be less than 200 fs, consistent with Ref. [27].

The data were also investigated for possible sources of systematic uncertainty. The sensitivity of the fits to the location of the targets was checked by varying the target positions by up to ± 1 mm along the beam axis in the simulations. This introduced an extra uncertainty of 11% in the final result. Stopping power tables were generated using SRIM [31] and an ATIMA subroutine built into LISE++ [32] and used in the Geant4 simulations to test the dependence on different stopping power models. This resulted in an uncertainty of 7% in the final lifetime. To evaluate the sensitivity of the lifetime to the background, which is slightly underpredicted in the Compton region in Fig. 2, different functional forms were evaluated and found to affect the lifetime at about the 5% level. In addition, a component was added to the simulations which corresponds to population of the 2_1^+ state by the 0_2^+ state, which produces an almost flat background that extends to 2100 keV. This did not significantly affect the measured lifetime, and was removed from the fit. The dependence of the excitation cross section on the

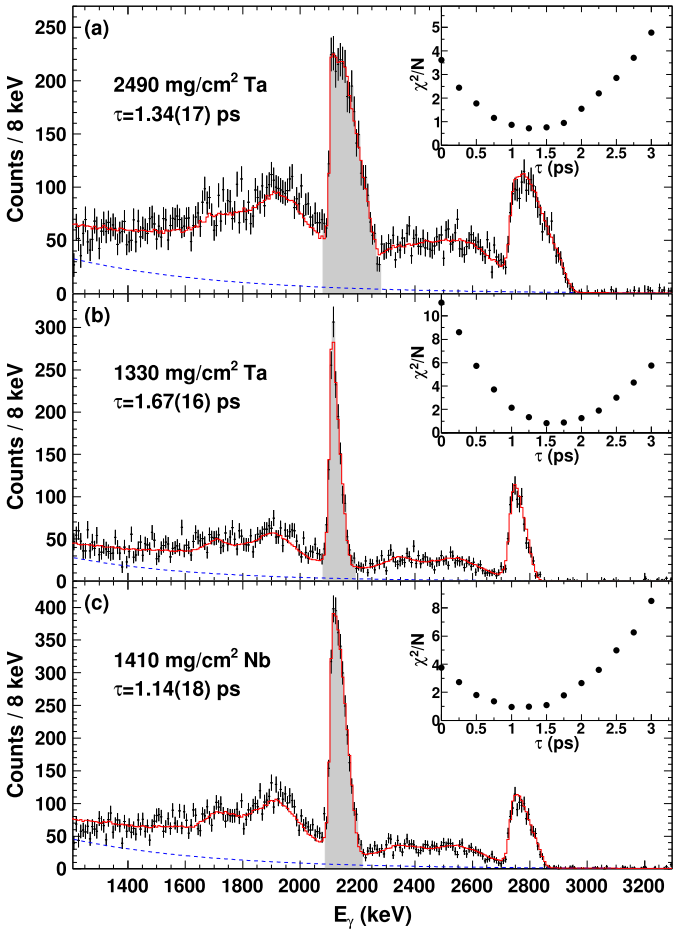

Fig. 2. (Color online) Simulations fit to the observed Doppler-corrected γ-ray spectrum for ^{12}Be; (a) the 2490-mg/cm^2 Ta target data; (b) the 1330-mg/cm^2 Ta target data; (c) the 1410-mg/cm^2 Nb target data. In each panel, the data is shown with error bars as the black crosses, the red line is the best-fit simulation with exponential background, and the background is shown separately as the dashed blue line. The shaded region under the peaks indicates the region fit to determine the lifetime. The insets for each panel show the reduced χ^2 value as a function of simulated 2_1^+-state lifetime.

changing beam energy in the targets was checked by comparing the observed γ-ray yield of the $1_1^- \rightarrow 0_1^+$ transition for the two tantalum targets. After accounting for the different number of ions observed with each target, the γ-ray yield scales exactly with the target thickness. From this, the excitation cross section is deduced to be essentially constant across the width of the targets, which is the same condition used in the simulations. Added in quadrature, the systematic effects contributed a total of 14% to the final uncertainty.

The possibility that a significant fraction of the incoming beam was in the isomeric 0_2^+ state was also investigated. If present, feeding of the 2_1^+ state could occur at any point along the beam line due to the long isomer lifetime, which would create an additional background. The 0_2^+ isomer content of the incoming ^{12}Be beam was evaluated by implanting the beam into a thick aluminum block inside GRETINA. A small number of 511-keV photons were observed from the $0_2^+ \rightarrow 0_1^+$ decay, and from this the isomer content of the beam was estimated to be about 0.5% at the S800 target position, which was neglected in the analysis. The at-rest decay of the 2_1^+ state was also observed in these data, which allowed confirmation of the γ-ray energy of this transition. The 2_1^+-state energy was found to be 2109(1) keV, which was used in the simulations and which is in good agreement with 2107(3) keV as reported in

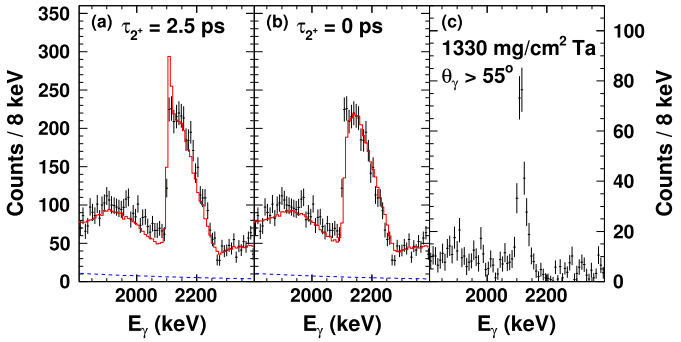

Fig. 3. (Color online) A comparison of a simulated γ-ray spectrum (red solid line) with a 2_1^+-state lifetime of (a) 2.5 ps and (b) 0 ps to the Doppler-corrected γ-ray spectrum from the 2490 mg/cm^2 Ta target measured in this work (black crosses). The simulation clearly does not reproduce the data in either case; for the 0 ps case, the low-energy edge is badly underpredicted where the decay in vacuum would be present, while for the 2.5 ps simulation there is a narrow peak at the low-energy edge of the photopeak from decay of the excited states after exiting the target which is not present in the data. This demonstrates that the lifetime of the 2_1^+ state is significantly shorter than 2.5 ps, but is not zero. (c) Data from the 1330 mg/cm^2 Ta target, with the γ-ray emission angle restricted to $\theta_\gamma > 55°$. This peak has a resolution of about 1.2%, which demonstrates that the resolution in this experiment is sufficient to generate the after-target peak in panel (a).

Ref. [20]. Taking the mean of the lifetime values measured for the three targets and accounting for the uncertainties discussed, the final result for the 2_1^+-state lifetime of ^{12}Be was determined to be $\tau_{2_1^+} = 1.38 \pm 0.10(\text{stat}) \pm 0.19(\text{sys})$ ps.

4. Discussion

On first inspection, it would appear that the previously determined lifetime value of $\tau_{2_1^+} = 2.5 \pm 0.7(\text{stat}) \pm 0.3(\text{sys})$ ps [20] is inconsistent with the value determined in this work. However, the range of lifetimes determined in the previous work spans from 1.1 ps to 3.9 ps within the 2σ uncertainty limits, encompassing the present result. In that light, the present result does not contradict the previous one; rather, it provides a much more precise determination of the lifetime which is useful for interpreting the structure of ^{12}Be. This fact notwithstanding, the present work is significant in that it demonstrates that the lifetime of the 2_1^+ state is considerably shorter than previously thought, and does not support a lifetime of 2.5 ps. This can be shown by comparing a simulation of the $2_1^+ \rightarrow 0_1^+$ transition with a lifetime of 2.5 ps to the data. This is most clearly seen with the thick-target tantalum data, shown in Fig. 3(a). The simulation in this case clearly does not match the data, with a prominent peak at low energies due to decay of the excited ^{12}Be nuclei after exiting the target. Fig. 3(b) shows a simulation with a lifetime of 0 ps; in contrast to the simulation in panel (a), the low-energy side of the peak is underestimated due to a lack of decays after the target, which shows that the lifetime is not consistent with zero. This comparison demonstrates that the lifetime is considerably shorter than previously reported, but still within the limits of this method. Finally, Fig. 3(c) shows data from the 1330 mg/cm^2 Ta target, restricted to angles greater than 55°. This represents the data which has the least sensitivity to the spread in the velocity in the Doppler-shift corrections, and has a full-width at half-maximum of about 26 keV. This corresponds to a resolution of about 1.2%, which compares well with the resolution of 0.9% obtained in Ref. [25]. While this data is not very sensitive to the lifetime of the 2_1^+ state, it does demonstrate that this experiment has sufficient resolution to produce a well-defined after-target peak if one existed, such as in the simulation in Fig. 3(a).

From the lifetime measured in this work, the transition probability is calculated to be $B(E2; 2_1^+ \rightarrow 0_1^+) = 14.2 \pm 1.0(\text{stat}) \pm 2.0(\text{sys})\ e^2\,\text{fm}^4$. The present result increases the $B(E2)$ value by about 80% compared to the previous value and reduces the relative uncertainty from about 30% to about 15%. With this revision it becomes clear that the ^{12}Be $B(E2)$ value is indeed larger than that of ^{10}Be ($B(E2) = 9.2(3)\ e^2\,\text{fm}^4$ [21]), increasing substantially despite being located at the traditional magic number $N = 8$. This change is consistent with the expectation that the $B(E2)$ is anti-correlated with the 2_1^+-state energy, as the fall in the $E(2_1^+)$ at ^{12}Be is now matched by a rise in the $B(E2)$. This resolves the ambiguity concerning the behavior of the beryllium isotopes at the shell closure; now all observables consistently indicate a breakdown of the $N = 8$ magic number.

The increased $B(E2)$ reported here indicates that ^{12}Be is significantly more collective than previously thought. This is in qualitative agreement with the findings of a recent laser spectroscopy measurement of the beryllium isotopes, which found that the RMS charge radius of ^{12}Be is 6% larger than that of ^{10}Be and attributed this change to an increase in the distance between the two α-clusters [8]. As a very simple discussion, we introduce a toy model wherein the beryllium isotopes consist of two charged point-particles to represent the α-clusters. In this model, the quadrupole moment can be written down as

$$Q_0 = \sum_q qr^2 = 2(Z_\alpha r^2) = 4er^2,$$

where r is the distance from the center of mass of the nucleus to one α-cluster. Then the $B(E2)$ takes the form

$$B(E2; 2_1^+ \rightarrow 0_1^+) = \frac{Q_0^2}{16\pi} = \frac{e^2}{\pi} r^4.$$

With $B(E2) = 14.2(22)\ e^2\,\text{fm}^4$ as found here, the radius at which the cluster centers can be found in ^{12}Be is calculated to be $r = 2.58(10)$ fm, which agrees well with the RMS charge radius of $R_c = 2.503(15)$ fm measured in Ref. [8]. Similarly for ^{10}Be, the measured value of $B(E2) = 9.2(3)\ e^2\,\text{fm}^4$ [21] gives $r = 2.32(2)$ fm, consistent with $R_c = 2.361(24)$ fm [8]. Although this is an oversimplified description of the beryllium isotopes, it is remarkable that such a simple toy model gives a reasonable description of the relationship between the measured $B(E2)$ values and the RMS charge radii for these isotopes. While it is difficult to conclude definitively that clustering is present in ^{12}Be from this discussion, it does suggest that ^{12}Be may be deformed, which could give rise to the enhanced $B(E2)$ observed in this work.

A number of theoretical investigations of ^{12}Be have included calculations of the $B(E2; 2_1^+ \rightarrow 0_1^+)$ transition rate and can be compared to the present measurement. Fig. 4 shows the results of several calculations (solid circles), as well as the previous and present experimental results for the $B(E2)$ shown as open and closed squares, respectively. The gray bands show the 1σ uncertainty range for each experimental result. The models used to calculate the theoretical results include Fermionic Molecular Dynamics (FMD) [8], No-Core Configuration Interaction (NCCI) [33], the Hyperspherical Adiabatic Expansion method (HSAE) [34], the No-Core Shell Model using CD-Bonn and "Inside Nonlocal Outside Yukawa" (INOY) interactions [35], the Generator Coordinate Method (GCM) [35], and Antisymmetrized Molecular Dynamics (AMD) [36]. Notably, the best agreement with the present result comes from the GCM and AMD results. Both of these calculations produce a pronounced cluster structure consisting of two helium nuclei, with the GCM beginning with ^{6}He–^{6}He and ^{8}He–^{4}He wave functions. In contrast, the remaining models underpredict

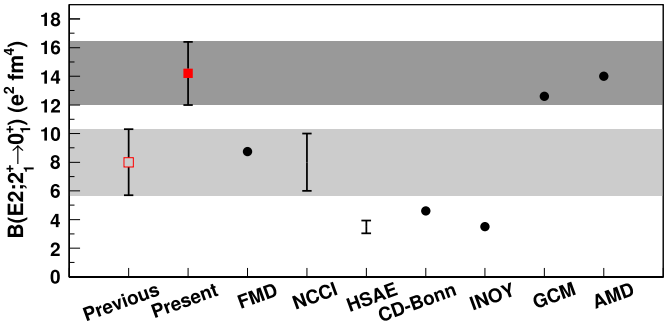

Fig. 4. (Color online) A comparison of the previous (open square) [20] and present (closed square) experimental $B(E2)$ values to theoretical predictions (solid circles or vertical ranges). The shaded bands show the experimental uncertainties. Theoretical values were generated using Fermionic Molecular Dynamics (FMD) [8], No-Core Configuration Interaction (NCCI) [33], Hyperspherical Adiabatic Expansion (HSAE) [34], No-Core Shell Model (CD-Bonn and INOY) [35], Generator Coordinate Method (GCM) [35], and Antisymmetrized Molecular Dynamics (AMD) [36].

the $B(E2)$ reported here. The FMD calculation is the exception, as it does show clustering but somewhat underpredicts the present $B(E2)$. The authors of that study note that the transition rate is very sensitive to mixing between different configurations in their calculation, which is in turn sensitive to a phenomenological correction factor which acts as a surrogate for missing 3-body interactions. As the details of $3N$ forces are still being investigated, it may be that a slight adjustment of this correction factor would more fully capture the effects of three-body forces, which are not yet fully-known.

As a final discussion, it is interesting to note that the only model shown in Fig. 4 to explicitly include a microscopic three-body interaction (the AMD [36] calculation, which includes a zero-range three-body force) comes closest to reproducing the $B(E2)$ value reported in this work. Electromagnetic transition rates can be quite sensitive to small changes in nuclear wave functions, which makes them good testing grounds for various *ab initio* theories which may include three-body interactions. Particularly for strongly-clustered nuclei like the beryllium isotopes, $3N$ forces may play an important role in these calculations due to the cluster regions, which have a relatively high density. Recent investigations of ^{8}Be [37] and ^{10}Be [21] have been undertaken to precisely measure $E2$ transition rates and compare them to Green's Function Monte Carlo (GFMC) calculations, providing a strong test of various models which include $3N$ interactions. For $A = 12$ nuclei, GFMC is still challenging, with ^{12}C only recently becoming possible [38]. When such calculations become computationally feasible for ^{12}Be, the present measurement can serve as an important benchmark for these *ab initio* models.

In conclusion, we have performed a new measurement of the lifetime of the 2_1^+ state of ^{12}Be. We use the Doppler-Shift Attenuation Method at intermediate beam energies with several target materials in order to control for systematic effects. We find a lifetime of $\tau_{2_1^+} = 1.38 \pm 0.10(\text{stat}) \pm 0.19(\text{sys})$ ps, which provides a significant improvement in the precision of this observable. The corresponding increase in the $E2$ transition rate brings the $B(E2)$ and $E(2_1^+)$ systematics of the beryllium isotopes into agreement, demonstrating the dissolution of the $N = 8$ shell closure as reported in numerous recent works.

Acknowledgements

This work was supported by the U.S. Department of Energy, Office of Nuclear Physics, under Grant DE-FG02-94ER40848 and Contract No. DE-AC02-98CH10886, and the DOE National Nuclear Security Administration under Award No. DE-NA0000979. GRETINA

was funded by the DOE, Office of Science. Operation of the array at NSCL was supported by the National Science Foundation under Cooperative Agreement PHY-1102511 (NSCL) and DOE under Grant No. DE-AC02-05CH11231 (LBNL).

References

[1] J.A. Wheeler, Phys. Rev. 52 (1937) 1107.
[2] L.R. Hafstad, E. Teller, Phys. Rev. 54 (1938) 681.
[3] K. Ikeda, N. Takigawa, H. Horiuchi, Prog. Theor. Phys. Suppl. E 68 (1968) 464.
[4] P. Maris, M.A. Caprio, J.P. Vary, Phys. Rev. C 91 (2015) 014310.
[5] Y. Kanada-En'yo, Phys. Rev. C 91 (2015) 014315.
[6] N. Ashwood, et al., Phys. Lett. B 580 (2004) 129.
[7] T. Neff, H. Feldmeier, R. Roth, Nucl. Phys. A 752 (2005) 321.
[8] A. Krieger, et al., Phys. Rev. Lett. 108 (2012) 142501.
[9] J.G. Johansen, et al., Phys. Rev. C 88 (2013) 044619.
[10] M. Freer, et al., Phys. Rev. Lett. 82 (1999) 1383.
[11] R. Kanungo, et al., Phys. Lett. B 682 (2010) 391.
[12] J. Benn, E. Dally, H. Müller, R. Pixley, H. Staub, H. Winkler, Nucl. Phys. A 106 (1967) 296.
[13] W. von Oertzen, M. Freer, Y. Kanada-En'yo, Phys. Rep. 432 (2006) 43.
[14] T. Moriguchi, et al., Nucl. Phys. A 929 (2014) 83.
[15] F. Ajzenberg-Selove, Nucl. Phys. A 506 (1990) 1.
[16] F. Ajzenberg-Selove, Nucl. Phys. A 413 (1984) 1.
[17] H. Iwasaki, et al., Phys. Lett. B 481 (2000) 7.
[18] A. Navin, et al., Phys. Rev. Lett. 85 (2000) 266.
[19] S.D. Pain, et al., Phys. Rev. Lett. 96 (2006) 032502.
[20] N. Imai, et al., Phys. Lett. B 673 (2009) 179.
[21] E.A. McCutchan, et al., Phys. Rev. Lett. 103 (2009) 192501.
[22] S. Paschalis, et al., Nucl. Instrum. Methods A 709 (2013) 44.
[23] D.J. Morrissey, B.M. Sherrill, M. Steiner, A. Stolz, I. Wiedenhoever, Nucl. Instrum. Methods B 204 (2003) 90.
[24] D. Bazin, J.A. Caggiano, B.M. Sherrill, J. Yurkon, A. Zeller, Nucl. Instrum. Methods B 204 (2003) 629.
[25] D. Weisshaar, et al., Nucl. Instrum. Methods A 847 (2017) 187.
[26] S. Shimoura, et al., Phys. Lett. B 654 (2007) 87.
[27] H. Iwasaki, et al., Phys. Lett. B 491 (2000) 8.
[28] P. Adrich, D. Enderich, D. Miller, V. Moeller, R.P. Norris, K. Starosta, C. Vaman, P. Voss, A. Dewald, Nucl. Instrum. Methods A 598 (2009) 454.
[29] S. Agostinelli, et al., Nucl. Instrum. Methods A 506 (2003) 250.
[30] R. Brun, F. Rademakers, Nucl. Instrum. Methods A 389 (1997) 81.
[31] J.F. Ziegler, M. Ziegler, J. Biersack, Nucl. Instrum. Methods B 268 (2010) 1818.
[32] O. Tarasov, D. Bazin, Nucl. Instrum. Methods B 266 (2008) 4657.
[33] P. Maris, J. Phys. Conf. Ser. 445 (2013) 012035.
[34] C. Romero-Redondo, E. Garrido, D.V. Fedorov, A.S. Jensen, Phys. Rev. C 77 (2008) 054313.
[35] M. Dufour, P. Descouvemont, F. Nowacki, Nucl. Phys. A 836 (2010) 242.
[36] Y. Kanada-En'yo, H. Horiuchi, Phys. Rev. C 68 (2003) 014319.
[37] V.M. Datar, S. Kumar, D.R. Chakrabarty, V. Nanal, E.T. Mirgule, A. Mitra, H.H. Oza, Phys. Rev. Lett. 94 (2005) 122502.
[38] A. Lovato, S. Gandolfi, J. Carlson, S.C. Pieper, R. Schiavilla, Phys. Rev. Lett. 117 (2016) 082501.